CHEMISTRY OF MATERIALS

ARTICLE

pubs.acs.org/cm

# Diameter-Controlled Solid-Phase Seeding of Germanium Nanowires: Structural Characterization and Electrical Transport Properties

Sven Barth,[†,§] Maria M. Koleśnik,[‡,||] Keith Donegan,[†,‡] Vojislav Krstić,[‡,||] and Justin D. Holmes*[,†,‡]

[†]Materials and Supercritical Fluids Group, Department of Chemistry and the Tyndall National Institute, University College Cork, Cork, Ireland

[‡]Centre for Research on Adaptive Nanostructures and Nanodevices (CRANN), Trinity College Dublin, Dublin 2, Ireland

[§]Institute for Materials Chemistry, Vienna University of Technology, 1060 Vienna, Austria

[||]School of Physics, Trinity College Dublin, Dublin 2, Ireland

Supporting Information

**ABSTRACT:** Despite the huge progress recently made in understanding the phenomena of metal-promoted growth of one-dimensional (1D) semiconductors, the controlled formation of small diameter semiconductor nanowires is still challenging. Liquid growth promoters, such as the low melting Au/Ge eutectic, allow control of the aspect ratio, diameter, and structure of 1D crystals via external parameters, such as precursor feedstock, temperature, and operating pressure. However, the incorporation of metal atoms during the growth process, size variations of the nanowires due to agglomeration of the nucleating metal seeds, and surface diffusion of Au via the vapor−liquid−solid route have been reported. Here, we detail the influence of solid growth seeds, such as $NiGe_2$ formed from Ni nanoparticles, on the lateral dimensions of Ge nanowires grown using a supercritical fluid growth process. Beneficial control over the mean nanowire diameter, in the sub-20 nm regime, with a predominantly ⟨110⟩ growth direction and low structural defect concentration was obtained using Ni seeds. In addition, the effect of prealloying of Ni−Fe films for the growth of Ge nanowires was investigated, which leads to a bimodal nanowire distribution. Electrical characterization performed on single nanowire devices showed p-type behavior for Ge nanowires grown from Ni and Ni/Fe seeds. Determination of resistivities, majority carrier concentrations, and mobilities suggest significant doping of the Ge nanowires by Ni when grown via a supercritical fluid−solid−solid (SFSS) mechanism.

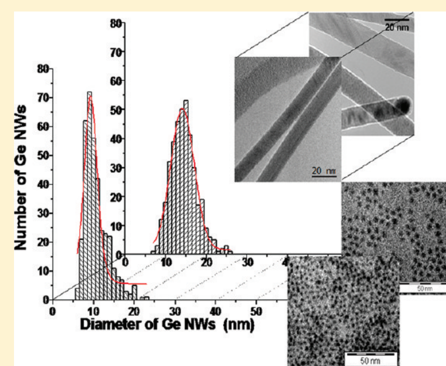


**KEYWORDS:** germaniumn, nanowire, solid-phase-seeding, SFSS, nickel

One-dimensional (1D) semiconductor nanostructures are promising components for a broad range of current and future applications.[1,2] Manipulation of the chemical and physical properties of semiconductor nanowires is achievable through careful control of their morphology, dimensions, crystallographic phase, and orientation. The application portfolio for semiconductor nanowires includes energy harvesting[3] and generation,[4] sensing,[5] optics,[6] and electronics.[7] Nonmetal-containing approaches for growing Ge nanowires include oxide-assisted growth,[8] impurity catalyzed formation,[9] or self-seeding.[10] In addition, several metal supported/catalyzed-growth mechanisms, such as vapor−solid−solid (VSS),[11] vapor−liquid−solid (VLS),[12] supercritical-fluid−liquid−solid (SFLS),[13] and supercritical-fluid−solid−solid (SFSS)[14] have been used to describe and interpret the growth of 1D nanostructures by vapor, liquid, and supercritical fluid phase techniques.

The solid-phase seeding of semiconductor nanowires usually requires lower synthesis temperatures compared to VLS growth but using the same seed material, leading to supposedly minimal contamination of the semiconductor; as both the diffusivity and equilibrium solubility of metals in semiconductors increases with temperature.[15] Solid-phase seeding potentially suppresses the unintentional incorporation of high dopant concentrations observed in semiconductor nanowires by the seed material for VLS growth.[16] In addition, compositional tailing observed at the interfaces of segmented Group 14 semiconductor heterostructures grown using liquid Au particles[17] was suppressed, leading to the formation of very sharp interfaces between segments grown by a VSS process.[18] The growth of sub-20 nm Si nanowires has also been demonstrated via a solid particle-based process by chemical vapor deposition.[19] The superior size retention of metal seeds in a VSS[20] and SFSS[21] process, when compared to a procedure using Au colloids has been described in the literature. The exciton Bohr radius, which is a good benchmark below which quantum confinement effects should be observed, is 24.3 nm for Ge.[22] However, prominent quantum effects are expected to be present far below this critical value. Therefore, the challenge is to control the nanowire diameter of Ge in the sub-

**Received:** March 3, 2011
**Revised:** June 14, 2011
**Published:** June 30, 2011

ACS Publications © 2011 American Chemical Society

20 nm range.[23] We recently demonstrated the excellent size control of Ge nanowire cores below 10 nm using a precursor which reduces the diffusion speed of Ge species and leads to core−shell structures with very narrow Ge nanowire core diameters.[10] To date, a variation of the Ge nanowire radial dimensions by solid-phase seeding and electrical characterization of Ni-seeded Ge nanowires has not been reported in literature.

Here, we describe the size-selective SFSS formation of 1D Ge nanostructures, using Ni as growth promoter, and growth via Ni/Fe mixtures acting as seed material. In addition, we report on the electrical transport characteristics of the nanowires synthesized. Nickel-promoted Ge nanowire formation was achieved using 3.0 (±0.5) nm and 4.4 (±0.6) nm nanoparticles obtained by the thermal decomposition of nickel acetyl-acetonate in high boiling point solvents in the presence of trioctylphosphine, which acts as a surfactant as shown in the Supporting Information (Figure S1). Oleylamine was used both as a reducing agent and as an intermediate ligand in the synthesis of the Ni nanoparticles in the targeted size regime as reported by Park et al.[24] The nanowire growth temperature was varied between 390 and 450 °C, which was high enough to ensure sufficient nanowire seeding via the SFSS mechanism. Higher temperatures were avoided with the catalytic Ni seeds to prevent the formation of amorphous shells surrounding the nanowires and the secondary nucleation of particles due to the kinetically enhanced thermal decomposition of the diphenylgermane precursor at elevated temperatures. The scanning electron microscopy (SEM) image in panel (a) of Figure 1 shows a high density of 1D Ge nanowires, with a low diameter distribution, which were determined by TEM to be in the diameter range between 9.3 (±1.6) nm and 14.2 (±2.8) nm grown at 410 °C on a Si substrate using Ni nanoparticles as a growth promoter. The Ni nanoparticles were originally capped with trioctylphosphine and adhered to the underlying silicon surface. Prior to the growth of Ge nanowires, some of the surfactant molecules detach during the drying procedure at elevated temperatures and low pressures, preventing the seeds from detaching from the substrate surface. The adsorption of Ni crystals onto a substrate is not necessary for growing Ge nanowires; however, the adsorption of the Ni seeds make it easier to collect the Ge nanowires at the end of a reaction, as well as allowing site-selective formation of the nanowires. Agglomeration or sintering of the Ni nanoparticles at elevated temperatures, leading to bigger catalytic seeds, was not observed in our experiments, which is a major advantage when compared to Ge nanowire growth using Au nanoparticle seeds.[21] Ni has a very high melting temperature and is stable against coarsening at temperatures employed in these studies.[25] The 1D Ge crystals were characterized by high resolution transmission electron microscopy (HRTEM). The majority of the product was highly crystalline as shown in panel (b) of Figure 1, and the defect density in the nanowires was low (approximately 2−5% of the wires exhibited multiple twinning events as shown below). The observed growth directions, determined by the corresponding FFT pattern of the HRTEM images, are displayed in Figure S2 of the Supporting Information for the Ge nanowires grown from the Ni nanocrystals. For Ge nanowire diameters below 20 nm,[26,27] the ⟨110⟩ orientation of the Ge crystals was predominant (>75%), with minor quantities of ⟨211⟩ and ⟨111⟩ also being present. The observation of a preferred ⟨110⟩ growth direction differs from data previously reported for Ni-seeded Ge nanowires grown under supercritical conditions, which described a similar quantity of ⟨111⟩ and ⟨110⟩ oriented Ge crystals.[21] Our

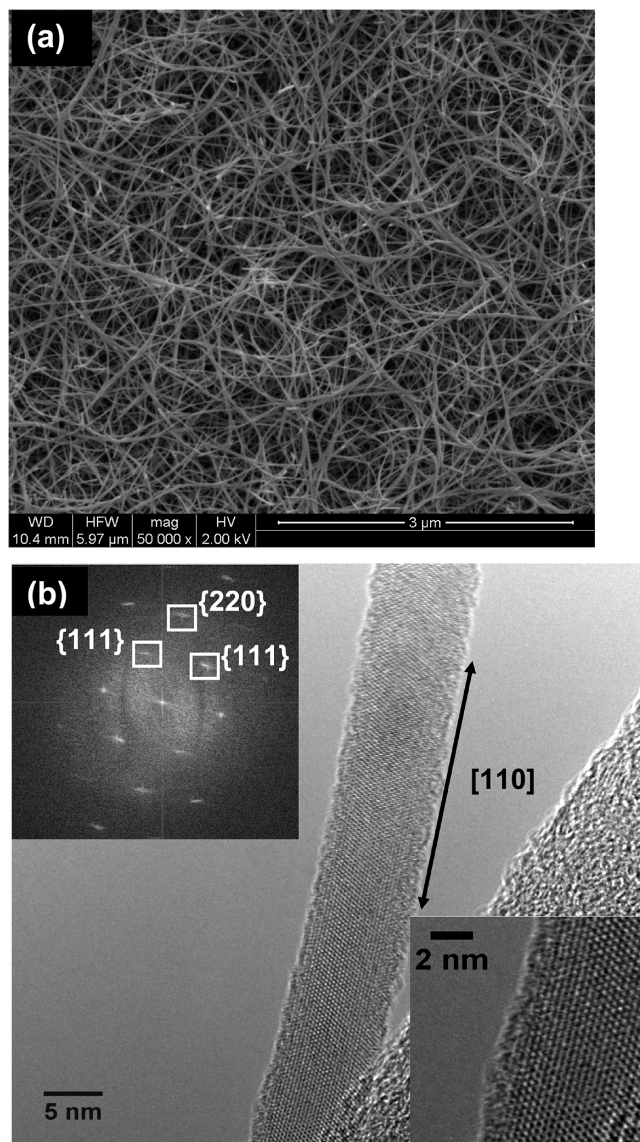


**Figure 1.** (a) SEM image illustrating the high density 1D Ge nanostructures grown from Ni nanoparticles. The HRTEM image shown in panel (b) represents a highly crystalline nanowire with a ⟨110⟩ growth direction (inset in panel (b) shows the high crystal quality of the nanowires synthesized).

studies show an expansion of the radial nanowire dimension of approximately 300−400% compared to the original size of the Ni nanoparticles. This observation is in agreement with the formation of a $NiGe_2$ seed prior to nanowire growth, which was also determined by EDX as shown in panel (a) of Figure 2. An FFT pattern obtained from a HRTEM image of a seed, as shown in panel (b) of Figure 2, also agrees with the lattice spacing of $NiGe_2$ (exp. 0.376 nm {111}; theor. 0.381 nm {111}).[28] The increase in the diameter of the initial Ni seed particles is primarily due to alloying of the Ni and Ge before the nucleation of the nanowires. As for most systems, the seed particle will be saturated with the decomposing material, and the most favored thermodynamically stable phase will form depending on the experimental conditions, which under our conditions will be the $NiGe_2$ alloy. The incorporation of two equivalents of Ge into the Ni lattice to form $NiGe_2$ is responsible for the increase in seed size and an

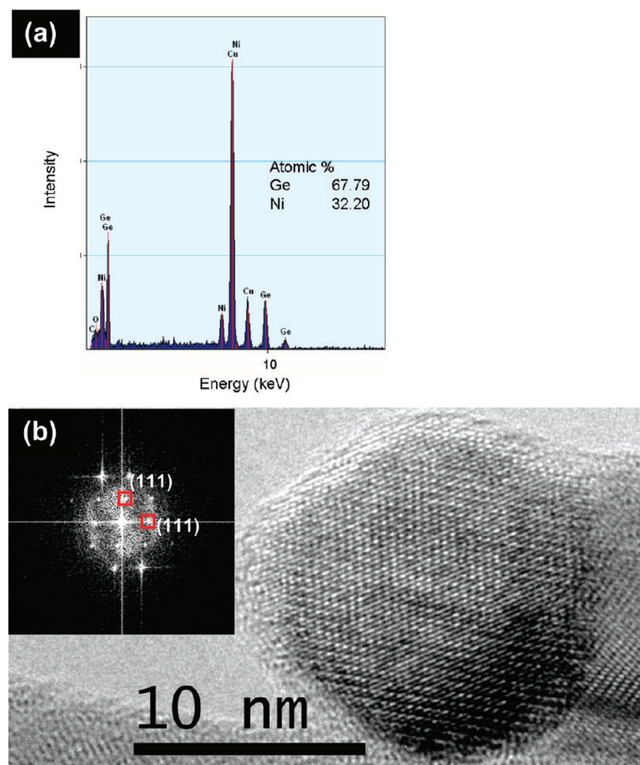


**Figure 2.** (a) Point EDX spectrum of a particle at the growth front of a Ge nanowire and reveals a 1:2 composition expected for $NiGe_2$. (b) HRTEM of a $NiGe_2$ growth seed showing a nonglobular shape and characteristic lattice spacing for $NiGe_2$ as determined by the corresponding FFT pattern (inset).

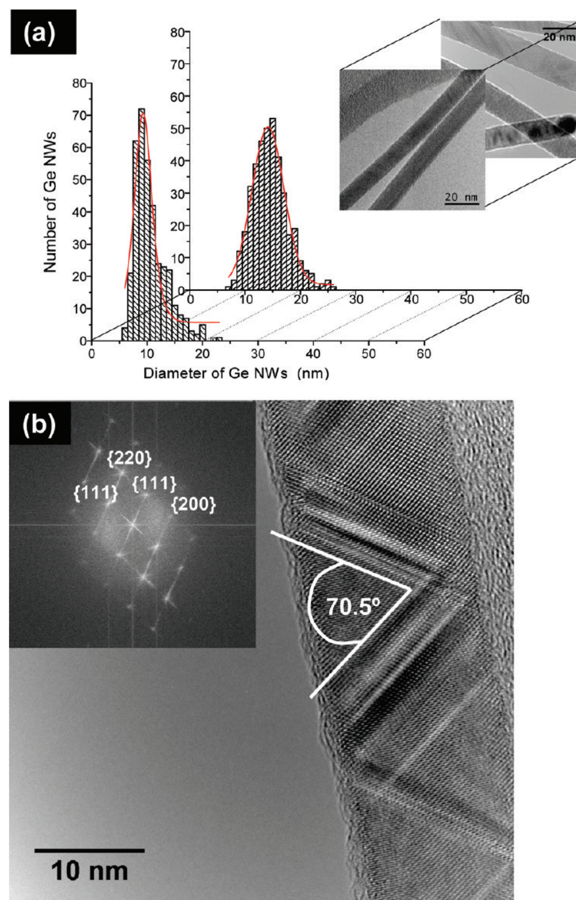


**Figure 3.** Graph in panel (a) illustrates the Ge nanowire diameter distributions obtained using Ni nanoparticles with mean diameters of 3.0 and 4.4 nm, obtained via a single peak fit of the diameter distribution data, and examples of TEM images used to determine the diameters of the nanowires. Mean nanowire diameters of 9.3 (±1.6) nm (front) and 14.2 (±2.8) nm (back) were obtained from the small and larger Ni seeds respectively. (b) TEM image of Ni seeded Ge nanowires revealing occasionally observed ⟨111⟩ stacking faults. Angles between stacking fault directions (70.5°) as well as between the stacking fault and the ⟨110⟩ growth direction (35.2°) are in agreement with theoretical orientations for cubic crystal structures.

intrinsic feature for the growth of nanowires when using metals which tend to form defined alloys as opposed to solid solutions where there is limited solubility of the decomposing species in the catalytic seed. The majority of the Ni seeds used in this study were single crystalline and exhibited nonhemispherical shapes after nanowire growth, leading to the conclusion that the seeds remained in a solid state while the Ge crystal was growing. During nanowire growth, the phase forming Ge species can either diffuse through the seed or migrate on the surface to the particle−substrate interface, where the particle usually exhibits the highest degree of curvature, leading to preferred nucleation sides.[29] Both scenarios probably coexist; however, the diffusion of Ge through the particles or Ni migration into the noncrystalline Ge is probably a major contribution. The existence of the Ge/Ni alloying process is identified by germanide formation as an initial step leading to an expansion of the seed size. These $NiGe_2$ alloy particles determine the diameter of the growing Ge crystals. Panel (a) of Figure 3 shows the diameter distributions for two types of nickel seeds used in our study. Ge nanowires with mean diameters of 9.3 (±1.6) nm and 14.2 (±2.8) nm were observed for 3.0 (±0.5) nm and 4.4 (±0.6) nm nickel seeds, respectively, as determined by analysis of the radial dimensions of the nanowires via TEM imaging (>350 nanowires per mean diameter were investigated). More examples of TEM images used to determine the mean nanowire diameters are shown in Figure S3 of the Supporting Information. In addition, the two histograms show the control of narrow diameter distributions in sub-20 nm Ge nanowires, synthesized from Ni nanocrystals with different mean diameters. The mean nanowire diameter is not exactly a multiple of the original seed size due to the orthorhombic nature of the $NiGe_2$ phase, and therefore, different degrees of expansion are expected along the a, b, and c axes.

In general, we observed a low structural defect density in the Ni-seeded Ge nanowires. Lamellar twinning along the wire axis was a minor feature due to a low density of ⟨112⟩ oriented Ge nanowires (<5%), in agreement with literature reports for Au- and Ni-seeded Ge nanowires.[21,30] Significant axial twinning has however been reported for Ag-seeded Ge nanowire growth.[31] Stacking faults observed in Ni-seeded thin Ge nanowires, which predominantly grew in the ⟨110⟩ direction, were of (111) type at a 35.2° angle to the growth direction and 70.5° with respect to each other as shown in panel (b) of Figure 3. These stacking faults run across the nanowires and are potentially nucleated due to surface/edge defects. The choice of the seed metal has a major impact on the formation of thin semiconductor nanowires via the SFSS approach and the structural properties of the grown nanowires.[31]

Attempts to grow Ge nanowires from sputtered pure Ni films were unsuccessful in our investigation, in the temperature range

 dx.doi.org/10.1021/cm200646e | *Chem. Mater.* 2011, 23, 3335–3340

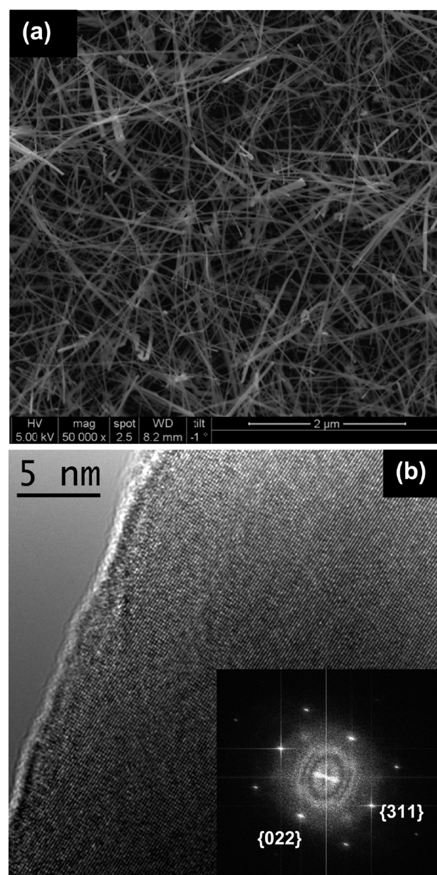


**Figure 4.** (a) SEM image of Ge nanowires grown from an Ni/Fe alloy coating shows a bimodal diameter distribution. The 1D materials are highly crystalline as shown in the HRTEM in panel (b) and the corresponding FFT.

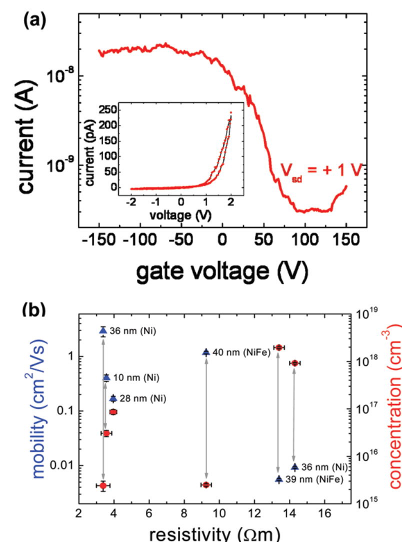


**Figure 5.** (a) Transfer and current−voltage characteristics of a 28 nm Ni-seeded nanowire showing p-type field-effect switching behavior. In the main figure a current-gate voltage curve taken at 1 V source−drain voltage is shown, exhibiting a strong increase in drain current for negative gate voltages. Inset: a typical I−V characteristic observed in both Ni- and Ni/Fe-seeded nanowire structures, with strong asymmetry and drain current increasing for positive voltages. (b) Carrier mobility and concentration values for Ni and NiFe seeded Ge nanowires as a function of the nanowire resistivity. The correlation between these parameters is a consequence of the acceptor properties of Ni and Fe impurities. For lower hole concentrations (below $10^{16}$ dopants per $cm^3$), the mobility values were observed to be much higher than those measured in structures with higher acceptor density (above $5 \times 10^{16}$ $cm^{-3}$), associated with a large increase in the number of trapping processes within the Ge bandgap.

between 390 and 420 °C, while a mixed deposit of iron and nickel films (~9:1, Ni:Fe) resulted in the growth of Ge nanowires with a bimodal diameter distribution as shown in panel (a) of Figure 4. This bimodal distribution of nanowire diameters is in accordance with studies reported for the growth of Ge nanowires from Cu/Ni films.[20] Similar to the Ni nanocrystal-seeded Ge nanowires, the 1D nanostructures grown from Ni/Fe films were highly crystalline as shown in panel (b) of Figure 4; however, the composition in the smaller and larger seeds differed from each other as determined by EDX analysis. According to the alloys expected for the pure transition metal germanides, the Ge content would be expected to exist as $MGe_2$ (M = Ni and Fe). Besides the expected germanium content in the particle at the tip of the nanowires, we found equal amounts of Ni and Fe in the particles of the smaller diameter fraction, with a mean diameter of approximately 30 (±10) nm. The binary seed alloy composition could be the most preferred composition for wires grown at 400−420 °C because of the formation of a fcc alloy from coexisting bcc Fe and the $FeNi_3$ phase at an eutectoid temperature of 359 °C (52.3% Ni), as shown in the Ni/Fe phase diagram.[32] EDX analysis of the larger crystals at the tip of large diameter Ge nanowires revealed merely a few percent iron (<10% metal ratio) in the particles. These thick (100−150 nm) wires also showed more defect sites than the thinner nanowires. Local inhomogeneity in the initial Ni/Fe film due to the sputtering process could be responsible for the two phases observed in the large and small particles found at the tips of the Ge nanowires. In addition, there might be an impact of the Ge species in the ternary alloy formation during nucleation of Ge nanowires, which might kinetically favor fcc particles over the formation of $MGe_2$ particles.

In order to investigate the characteristics of the charge-carrier transport in the nanowires, individual nanowires were contacted with Pd electrodes in a four-point configuration, via combined optical and electron-beam lithography. Prior to contacting, the nanowires were sonicated in toluene, and a small volume (5−20 μL) of the resulting nanowire suspension was dropped onto a thermally grown $SiO_2$ layer (300 nm). The underlying highly doped Si wafer was used as a back gate to investigate the field effect transistor (FET) behavior of the nanowires.[33] A typical contact configuration used in our investigations is shown in the inset of Figure 5. Current−voltage and transfer-characteristics were investigated for nanowires in the diameter range between 10 to 45 nm. Four-point measurements were carried out to determine resistivity values for individual nanowires and field-effect measurements in two-point configuration to determine the mobility independently (see section E of the Supporting Information).

All samples investigated, for both Ni- and Ni/Fe-seeded nanowires, revealed unipolar, p-type transfer characteristics along with nonlinear, asymmetric current−voltage curves, as shown for a Ni-seeded Ge nanowire in panel (a) of Figure 5. Generally some hysteresis was observed during the gate sweeps;[24,31] however, the characteristics remained fully reproducible. These electrical characteristics indicate that holes are the majority charge carriers in the nanowires. A p-type gate response could potentially be due to

catalyst incorporation in the nanowire, which acts as an electron acceptor,[34] intrinsic doping,[35] or surface effects due to oxidized species.[36] Four-point measurements revealed resistivity values ranged from 3.4 to 14.3 Ωm for the Ge nanowire devices measured, which is significantly higher than intrinsic bulk germanium (0.46 Ωm). The nanowire hole mobility, determined from the transfer characteristics, was found to be several orders of magnitude lower (~0.006−3 $cm^2\ V^{-1}\ s^{-1}$) than the value found in single-crystalline bulk germanium (1700 $cm^2\ V^{-1}\ s^{-1}$ (Ref 37)). The low mobilities obtained in the nanowires are in accordance with previous investigations on Si[38] and Ge[39] nanowires, which may be something to do with the spatial confinement of the charge carriers in quasi-1D nanostructures. The majority carrier (hole) concentrations in the nanowires were determined to be in the range between $2 \times 10^{15}$ and $5 \times 10^{18}$ atoms $cm^{-3}$. Both Ni and Fe are known to be fast diffusing species in Ge,[40] potentially leading to the incorporation of metal impurities in the growing Ge crystal. Consequently, Ni and Fe impurities can lead to the formation of deep, double acceptor levels within the Ge bandgap, with energies (in bulk) of $E_V$ = +0.22 eV and $E_C$ = −0.3 eV for Ni[41] and $E_V$ = +0.34 and $E_C$ = −0.27 eV for Fe,[42] respectively ($E_{V/C}$: valence/conduction band edge). Unintentional doping with Ni and Fe is the most likely explanation for the p-type behavior observed with the Ge nanowire devices. In addition, the carrier mobility is increasingly influenced by a charge-trapping mechanism at higher doping levels,[44] which for Ni and Fe in bulk germanium are expected to start to be active at ionized dopant levels of the order of $10^{15}$ atoms $cm^{-3}$ (ref 43) and $10^{13}$−$10^{14}$ atoms $cm^{-3}$ (ref 44), respectively.

EDX and EELS analysis on the germanium nanowires revealed no signal from Ni or Fe, setting an upper limit for the Ni and Fe atom concentration of approximately $2 \times 10^{20}$ atoms $cm^{-3}$, which corresponds to the resolution limit of the instruments (0.5% under optimum conditions; atom-density in germanium ~$4.4 \times 10^{22}$ $cm^{-3}$ at room temperature). Panel (b) of Figure 5 shows carrier concentration and field-effect mobility, corrected for contact-resistance contribution, (see Section E of the Supporting Information) of individual nanowires plotted as a function of nanowire resistivity, to illustrate the impact of this unintentional doping of the nanowires grown via the SFSS mechanism. High (above threshold) acceptor densities in transition metal-doped Genanowires will cause a redistribution of carrier capture and recombination processes and trap filling processes become dominant.[45] The charge-trapping mechanism associated with metal dopants in our nanowires influences the carrier drift, hence lowering the effective carrier mobility due to acceptor concentrations about the threshold level in all of the nanodevices investigated.[46] For nanowires with resistivities below 10 Ωm, the carrier concentration does not exceed $10^{17}$ atoms per $cm^3$, and the mobility values range from 0.17 to 3 $cm^2\ V^{-1}\ s^{-1}$. In contrast, nanowires with resistivities >10 Ωm have acceptor densities higher than $9 \times 10^{17}$ $cm^{-3}$, which are associated with significantly lower mobilities (0.006−0.009 $cm^2\ V^{-1}\ s^{-1}$). Hence, a less than 10-fold increase in the number of dopants in the nanowire body leads to a drop in the carrier mobility by 3 orders of magnitude.

Previous reports have investigated charge transport in SFLS-synthesized Ge nanowires catalyzed by Au seeds. The observation of p-type field effect characteristics and low hole mobility was attributed to the presence of strong charge traps on the nanowire surface and not the incorporation of Au into the nanowire body.[47,48] Even though the density of Au in the material was undetectable in VLS-grown nanowires,[49] the incorporation of gold acceptors into the nanowire body, which influences the transport properties, should not be neglected. In our study, we found that the hole mobility values can change over several orders of magnitude depending on the majority carrier concentration in the nanowires. It should be emphasized that all nanostructures measured were fabricated from the same nanowire batches (Ni and Ni/Fe) without surface modification on the same chip and with the same methods. However, the lack of any diameter-dependent transport parameters observed in our nanowires suggests that the field-effect response does not originate from the structure or composition of the surface capping layer.[35] Therefore, the hole transport in our Ge nanowires is most likely a direct consequence of transition metal doping.

Besides the presence of transition metal impurities in the Ge nanowires, further factors affecting the electrical performance of the nanostructures have been reported in the literature, such as scattering processes at the surface of the nanostructure[34] and at grain boundaries.[50] The presence of {111} stacking faults is already mentioned above. Surface scattering events should not be neglected in the determination of the electrical properties of our Ge nanowire devices; however, these are not dominating because no clear diameter dependence was observed. We are currently studying the effectiveness of surface treatments,[51] which will enable us to evaluate the electrical transport properties of thin sub-20 nm nanowires produced from colloidal Ni seeds to exclude surface contributions. Focusing more on the electrical characteristics of larger diameter nanowires in this paper, sub-20 nm nanowires synthesized by Ni nanoparticle seeds as described in the first part of the paper will be investigated to further understand the doping effect.

In summary, we have demonstrated the size selective growth of sub-20 nm Ge nanowires by solid-phase seeding using Ni nanocrystals in supercitical fluids. The nanowires are highly crystalline and showed a preferential ⟨110⟩ growth direction. Two different particle sizes enabled the growth of Ge nanowires with mean diameters of 9.3 and 14.2 nm, which is well below the Bohr radius for Ge and should theoretically enable the study of quantum effects. In addition, the influence of a Fe/Ni codeposited film acting as seed layer was evaluated for future studies on Ge nanowire growth. Electrical data obtained for these wires showed a p-type behavior associated with comparably low hole mobilities, which could be attributed to transition metal doping by Ni and Fe. These results demonstrate unintentional doping of Ge nanowires grown via a SFSS mechanism using Ni and Ni/Fe growth promoters.

## ■ ASSOCIATED CONTENT

**Supporting Information.** Detailed experimental methods and parameters, and TEM images of the size-selective Ge nanowire synthesis and Ni nanoparticles. This material is available free of charge via the Internet at http://pubs.acs.org.

## ■ AUTHOR INFORMATION

**Corresponding Author**

*E-mail: j.holmes@ucc.ie. Tel: +353 (0)21 4903608. Fax: +353 (0)21 4274097.

## ■ ACKNOWLEDGMENT

We acknowledge financial support from the Science Foundation Ireland (Grants 07/RFP/MASF710, 08/CE/I1432, and

08/IN.1/I1873). This research was also enabled by the Higher Education Authority Program for Research in Third Level Institutions (2007-2011) via the INSPIRE programme.

## ■ REFERENCES

(1) Barth, S.; Hernandez-Ramirez, F.; Holmes, J. D.; Romano-Rodriguez, A. *Prog. Mater. Sci.* **2010**, *55*, 563.
(2) Schmidt, V.; Wittemann, J. V.; Gosele, U. *Chem. Rev.* **2010**, *110*, 361.
(3) Kempa, T. J.; Tian, B. Z.; Kim, D. R.; Hu, J. S.; Zheng, X. L.; Lieber, C. M. *Nano Lett.* **2008**, *8*, 3456.
(4) Wang, Z. L.; Song, J. H. *Science* **2006**, *312*, 242.
(5) Hernandez-Ramirez, F.; Barth, S.; Tarancon, A.; Casals, O.; Pellicer, E.; Rodriguez, J.; Romano-Rodriguez, A.; Morante, J. R.; Mathur, S. *Nanotechnology* **2007**, *18*, 424016.
(6) Huang, M. H.; Mao, S.; Feick, H.; Yan, H. Q.; Wu, Y. Y.; Kind, H.; Weber, E.; Russo, R.; Yang, P. D. *Science* **2001**, *292*, 1897.
(7) Cui, Y.; Zhong, Z. H.; Wang, D. L.; Wang, W. U.; Lieber, C. M. *Nano Lett.* **2003**, *3*, 149.
(8) Zhang, A.; Kim, H.; Cheng, J.; Lo, Y. H. *Nano Lett.* **2010**, *10*, 2117.
(9) Kazakova, O.; Van Der Meulen, M. I.; Petkov, N.; Holmes, J. D. *IEEE Trans. Magn.* **2009**, *45*, 4085.
(10) Hobbs, R. G.; Barth, S.; Petkov, N.; Zirngast, M.; Marschner, C.; Morris, M. A.; Holmes, J. D. *J. Am. Chem. Soc.* **2010**, *132*, 13742.
(11) Lensch-Falk, J. L.; Hemesath, E. R.; Perea, D. E.; Lauhon, L. J. *J. Mater. Chem.* **2009**, *19*, 849.
(12) Miyamoto, Y.; Hirata, M. *Jpn. J. Appl. Phys.* **1975**, *14*, 1419.
(13) Hanrath, T.; Korgel, B. A. *J. Am. Chem. Soc.* **2002**, *124*, 1424.
(14) Tuan, H. Y.; Lee, D. C.; Hanrath, T.; Korgel, B. A. *Nano Lett.* **2005**, *5*, 681.
(15) Graff, K. *Metal Impurities in Silicon-Device Fabrication*; 2nd ed.; Springer: New York, 2000.
(16) Ke, Y.; Weng, X. J.; Redwing, J. M.; Eichfeld, C. M.; Swisher, T. R.; Mohney, S. E.; Habib, Y. M. *Nano Lett.* **2009**, *9*, 4494.
(17) Clark, T. E.; Nimmatoori, P.; Lew, K. K.; Pan, L.; Redwing, J. M.; Dickey, E. C. *Nano Lett.* **2008**, *8*, 1246.
(18) Wen, C. Y.; Reuter, M. C.; Bruley, J.; Tersoff, J.; Kodambaka, S.; Stach, E. A.; Ross, F. M. *Science* **2009**, *326*, 1247.
(19) Wittemann, J. V.; Munchgesang, W.; Senz, S.; Schmidt, V. *J. Appl. Phys.* **2010**, *107*, 096105.
(20) Kang, K.; Gu, G. H.; Kim, D. A.; Park, C. G.; Jo, M. H. *Chem. Mater.* **2008**, *20*, 6577.
(21) Tuan, H. Y.; Lee, D. C.; Hanrath, T.; Korgel, B. A. *Chem. Mater.* **2005**, *17*, 5705.
(22) Maeda, Y.; Tsukamoto, N.; Yazawa, Y.; Kanemitsu, Y.; Masumoto, Y. *Appl. Phys. Lett.* **1991**, *59*, 3168.
(23) Liang, G.; Xiang, J.; Kharche, N.; Klimeck, G.; Lieber, C. M.; Lundstrom, M. *Nano Lett.* **2007**, *7*, 642.
(24) Park, J.; Kang, E.; Son, S. U.; Park, H. M.; Lee, M. K.; Kim, J.; Kim, K. W.; Noh, H. J.; Park, J. H.; Bae, C. J.; Park, J. G.; Hyeon, T. *Adv. Mater.* **2005**, *17*, 429.
(25) Carenco, S.; Boissiere, C.; Nicole, L.; Sanchez, C.; Le Floch, P.; Mezailles, N. *Chem. Mater.* **2010**, *22*, 1340.
(26) Dailey, E.; Drucker, J. *J. Appl. Phys.* **2009**, *105*, 064317.
(27) Madras, P.; Dailey, E.; Drucker, J. *Nano Lett.* **2009**, *9*, 3826.
(28) Takizawa, H.; Uheda, K.; Endo, T. *J. Alloys Compd.* **2000**, *305*, 306.
(29) Cheyssac, P.; Sacilotti, M.; Patriarche, G. *J. Appl. Phys.* 2006, *100*,
(30) Hanrath, T.; Korgel, B. A. *Small* **2005**, *1*, 717.
(31) Barth, S.; Boland, J. J.; Holmes, J. D. *Nano Lett.* **2011**, *11*, 1550.
(32) Swartzendruber, L.; Itkin, V.; Alcock, C. *J. Phase Equilib.* **1991**, *12*, 288.
(33) Wunnicke, O. *Appl. Phys. Lett.* **2006**, *89*, 083102.
(34) Wang, J.; Polizzi, E.; Ghosh, A.; Datta, S.; Lundstrom, M. *Appl. Phys. Lett.* **2005**, *87*, 043101.
(35) Zhang, S.; Hemesath, E. R.; Perea, D. E.; Wijaya, E.; Lensch-Falk, J. L.; Lauhon, L. J. *Nano Lett.* **2009**, *9*, 3268.
(36) Wang, D.; Dai, H. *Appl. Phys. A: Mater. Sci. Process.* **2006**, *85*, 217.
(37) Haynes, J. R.; Shockley, W. *Phys. Rev.* **1951**, *81*, 835.
(38) Goldberger, J.; Hochbaum, A. I.; Fan, R.; Yang, P. D. *Nano Lett.* **2006**, *6*, 973.
(39) Yoo, B.; Dodabalapur, A.; Lee, D. C.; Hanrath, T.; Korgel, B. A. *Appl. Phys. Lett.* **2007**, *90*, 072106.
(40) Wei, L. Y. *J. Phys. Chem. Solids* **1961**, *18*, 162.
(41) Tyler, W. W.; Newman, R.; Woodbury, H. H. *Phys. Rev.* **1955**, *98*, 461.
(42) Tyler, W. W.; Woodbury, H. H. *Phys. Rev.* **1954**, *96*, 874.
(43) Clauws, P.; Simoen, E. *Mater. Sci. Semicond. Process.* **2006**, *9*, 546.
(44) Battey, J. F.; Baum, R. M. *Phys. Rev.* **1955**, *100*, 1634.
(45) Forment, S.; Vanhellemont, J.; Clauws, P.; Van Steenbergen, J.; Sioncke, S.; Meuris, M.; Simoen, E.; Theuwis, A. *Mater. Sci. Semicond. Process.* **2006**, *9*, 559.
(46) Yoon, Y.; Lin, J. S.; Pearton, S. J.; Guo, J. *J. Appl. Phys.* **2007**, *101*, 024301.
(47) Hanrath, T.; Korgel, B. A. *J. Am. Chem. Soc.* **2004**, *126*, 15466.
(48) Hanrath, T.; Korgel, B. A. *J. Phys. Chem. B* **2005**, *109*, 5518.
(49) Perea, D. E.; Hemesath, E. R.; Schwalbach, E. J.; Lensch-Falk, J. L.; Voorhees, P. W.; Lauhon, L. J. *Nat Nano* **2009**, *4*, 315.
(50) Durkan, C.; Welland, M. E. *Phys. Rev. B* **2000**, *61*, 14215.
(51) Collins, G.; Fleming, P.; Barth, S.; O'dwyer, C.; Boland, J. J.; Morris, M. A.; Holmes, J. D. *Chem. Mater.* **2010**, *22*, 6370.